



Flow and melting of a heterogeneous mantle: 2. Implications for a chemically nonlayered mantle

Garrett Ito*, John J. Mahoney

School of Ocean and Earth Science and Technology, POST 810, University of Hawaii, Honolulu, HI 96822, United States

Received 14 June 2004; received in revised form 1 September 2004; accepted 26 October 2004

Available online 25 December 2004

Editor: B. Wood

Abstract

We have recently examined the importance of upper mantle flow and melting of a heterogeneous mantle on the incompatible trace element and isotope composition of ocean island basalts (OIBs) and mid-ocean ridge basalts (MORBs) [G. Ito, J. Mahoney, Flow and melting of a heterogeneous mantle 1: method and importance to the geochemistry of ocean island and mid-ocean ridge basalts, *Earth Planet. Sci. Lett.* 230 (2005) 29–46]. We found that the combination of thicker lithosphere and enhanced mantle upwelling deep in the melting zone beneath hotspots can lead to many geochemical characteristics that distinguish OIBs from MORBs. These results occurred in the absence of any geochemical distinction between mantle plumes, which we assumed to feed OIB volcanism, and the upper mantle, which we assumed to feed MORB volcanism. Our findings renew the possibility for OIB and MORB geochemical systematics to arise out of a well-stirred heterogeneous mantle without large-scale layering. In this study, we test this possibility by solving for the mantle source compositions that, when melted in a hot plume beneath lithosphere of appropriate thickness, can explain key geochemical correlations at specific hotspots. Both the age of the seafloor at the time of volcanism and correlations between Sr, Nd, and Pb isotopes are considered in model fits to the OIB data. We then compute the magma composition that would arise out of these same mantle sources when melted at normal temperatures beneath a mid-ocean ridge. On one hand, some predicted MORB compositions lie outside the range of compositions represented by our collection of “normal” MORB data. This result is consistent with the conventional wisdom that mantle plumes sample a deep mantle layer that is compositionally distinct from the upper mantle. On the other hand, many solutions are indistinguishable from the observed MORB compositions and thus do not require a chemically layered mantle. Focusing on these solutions, the implied range of (nonlayered) mean mantle compositions can satisfy the global Th and U budget if the upper-bound estimates for the content of these elements in the continents are used. Our mean mantle produces only a small percentage (<~30%) of the mantle heat budget and therefore requires a large heat flux from the core. Such a condition can allow for reasonably low secular cooling rates if a thick dehydrated lithosphere has existed over the mantle’s history and has retarded global heat loss, as a recent study [J. Korenaga, Energetics of mantle convection and the fate of fossil heat, *Geophys. Res. Lett.* 30 (8), (2003) 1437, (doi:10.1029/2003GL016982)] suggests. Future tests for a nonlayered mantle should include integrated geodynamic and geochemical studies of correlations between noble gases and other isotopes, magma compositions at

* Corresponding author. Tel.: +886 808 956 9717; fax: +886 808 956 5154.

E-mail addresses: gito@hawaii.edu (G. Ito), jmahoney@hawaii.edu (J.J. Mahoney).

ultraslow spreading centers, and geographic variations in magma composition at hotspots, including those interacting with mid-ocean ridges.

© 2004 Elsevier B.V. All rights reserved.

Keywords: Mantle heterogeneity; Ocean island basalt (OIB); Mid-ocean ridge basalt (MORB); Mantle convection; Partial melting; mantle plume

1. Introduction

Trace element and radiogenic isotopic compositions of oceanic basalts indicate that geochemical heterogeneity in the mantle is long-lived ($>10^9$ yr) and exists over a wide range of length scales. At the largest scale, the mantle may be chemically stratified, as suggested by many workers to explain geochemical distinctions between ocean island basalts (OIBs) and mid-ocean ridge basalts (MORBs). Most commonly, an upper layer, characterized by long-term relative depletion in incompatible elements and having a relatively uniform composition, is postulated to feed mid-ocean ridge volcanism. A lower, more heterogeneous layer, containing variably depleted, primordial, and/or enriched material, is often thought to be delivered to the surface principally by mantle plumes (e.g., [3–8]). Mantle plumes are thought to incorporate deeply subducted material (e.g., [9–13]), lower mantle, and some upper mantle as they rise from thermal boundary layers (e.g., [14–16]) to the surface (e.g., [17–20]). At the same time, it is widely recognized that the mantle is also heterogeneous on scales smaller than typical volumes of melting zones in the upper mantle [21–29]. How significant this small-scale heterogeneity is compared to the large-scale heterogeneity associated with mantle layering is a general topic this study addresses.

A long-standing dilemma with the layered mantle hypothesis is presented by arguments for whole-mantle convection. Seismic studies show evidence for significant mass transfer between the upper and lower mantle via slab penetration (e.g., [30–33]), and geodynamic modeling [34,35] calls on whole mantle convection to explain global geophysical observations. Some geodynamic studies predict whole mantle convection to efficiently stir the mantle, finding it difficult to preserve large-scale chemical layers over G.y. times scales (e.g., [22,36–40]), whereas others conclude that compositionally dense material can

collect in the lower mantle and preserve mantle layering [41–45]. Such compositional layering, however, is predicted to have seismic structure in the midmantle that is not observed [44], implies an unrealistically high heat flux from the lower layer to the surface to be transported in mantle plumes (i.e., if the lower layer contains a large fraction of the mantle's heat-producing elements [46]), and does not readily explain the preservation of primitive material if the lower-layer material is primarily subducted oceanic crust, which would have degassed when it first formed at the surface.

Other solutions to this problem have been proposed [36,46], and one that we address here emphasizes the preservation of heterogeneities in small bodies [22,47–50]. Statistical methods [49,50] have shown that widespread heterogeneity can explain many aspects of the geochemical diversity among OIB and MORB, but the above studies do not explicitly address the distinctions between mean MORB and mean OIB compositions. In our recent manuscript [1], we examined the geochemical consequences of flow and melting of a heterogeneous mantle. Results showed that if different mantle components begin melting at different depths, a large diversity of trace element and isotope compositions can arise, depending on the thickness of the lithosphere as well as vertical variations in mantle upwelling and decompression in the melting zone. In fact, models predicted compositional ranges that spanned a large portion of both the OIB and MORB data fields without any inherent difference between the respective mantle sources. This result opens the possibility that many of the geochemical systematics of oceanic basalts arise out of a nonlayered, well-stirred heterogeneous mantle.

We examine this possibility in further detail. We begin with a short description of the data we have compiled, followed by a review of the essential aspects of our model. We then illustrate how a nonlayered

heterogeneous mantle can generate many incompatible trace element and isotope systematics of the global OIB and MORB data set. Using a simple grid search scheme, we examine the range of mantle sources that can explain specific Sr, Nd, and Pb isotope systematics of several individual hotspot island chains. These model sources are then melted under conditions expected at mid-ocean ridges to quantify how well the predicted MORB compositions overlap the observed MORB field. Some solutions require compositional distinctions between OIB and MORB sources and some do not. For those solutions that do not, we discuss the implications for a nonlayered mantle.

2. Data

The geochemical data to which we compare model predictions are taken from various oceanic hotspot island groups and mid-ocean ridges (see figure in Appendix A). The hotspot island data are principally from the GEOROC database (<http://georoc.mpch-mainz.gwdg.de>). Mid-ocean ridge data include data from the Mid-Atlantic Ridge (MAR), East Pacific Rise (EPR), the Carlsberg Ridge, and the Southwest, Southeast, and Central Indian Ridges, primarily from the PETDB database (<http://petdb.ldeo.columbia.edu/petdb/>). For the MORB data, we wish to include only those sections of mid-ocean ridges experiencing “normal” melting conditions. Defining “normal” is seldom straightforward; in fact this manuscript will question what should be considered a normal mantle composition. Here, we emphasize sections of mid-ocean ridges that are physically normal, considering only those MORBs sampled in the depth range of 2500–3500 m. This range is meant to eliminate potential regions with unusually high or low rates of crustal production, possibly related to anomalous mantle flow or temperatures. Hotspot–ridge interactions are obvious examples of where mantle flow and/or temperature are likely to be atypical. Thus, we also eliminate sections considered to be hotspot-influenced [51–55]. It is true that hotspot or plume influence is recognized on the basis of MORB geochemistry, a criterion we wish to avoid; but atypical physical conditions are also indicated at these sites by anomalously shallow ridge depths or structural linkages with off-axis volcanism.

3. Melting model

Our method of modeling the incompatible trace element and isotope composition of primary magmas derived from a heterogeneous source is detailed in [1], but the main assumptions are as follows (Fig. 1). Most of the mantle is composed of depleted mantle peridotite (DM—“depleted” refers to the concentration of incompatible trace elements relative to estimated primitive mantle). Enriched mantle peridotite (EM) and pyroxenite (PX) are present in veins or blobs, with characteristic dimensions small enough to maintain thermal equilibrium during melting but large enough to maintain the chemical distinctions between the lithologies [56,57]. In addition to differences in trace element and isotope composition, the three lithologies have different melting functions, with the onset of melting occurring for EM, PX, and DM, respectively, at progressively lower pressure. Trace element concentrations of the melt from each lithology are computed by integrating fractional melts derived from rock in which solid phases change with pressure and melt fraction. Magma compositions are the weighted average of compositions from each lithology.

A key factor that influences the weighting from each lithology is the speed U at which mantle exits the melting zone as a function of depth z . At mid-ocean ridges, seafloor spreading drives an asthenospheric corner flow, with material exiting the melting zone at rate $U(z)$, which is approximately uniform and equal to the half-spreading rate. In a given increment of time, mid-ocean ridge melting generates a residual mantle column (RMC) of uniform width (Fig. 1). We assume that OIBs are generated by mantle plumes, where “plume” refers to a narrow buoyant upwelling (Fig. 1) but implies nothing about the depth of origin or chemistry of the upwelling material. In contrast to mid-ocean ridge flow, mantle plume flow is driven by deep-seated buoyancy; consequently, $U(z)$ is maximum at the base of the melting zone and decreases to zero at the base of the lithosphere. In a given increment of time, melting of an axisymmetric plume will generate a residual mantle cylinder (also RMC) that widens as a function of depth.

Compared to mid-ocean ridge flow, plume flow tends to more strongly weight melts derived from the deeper parts of the melting zone—melts that tend to be most concentrated in incompatible elements and

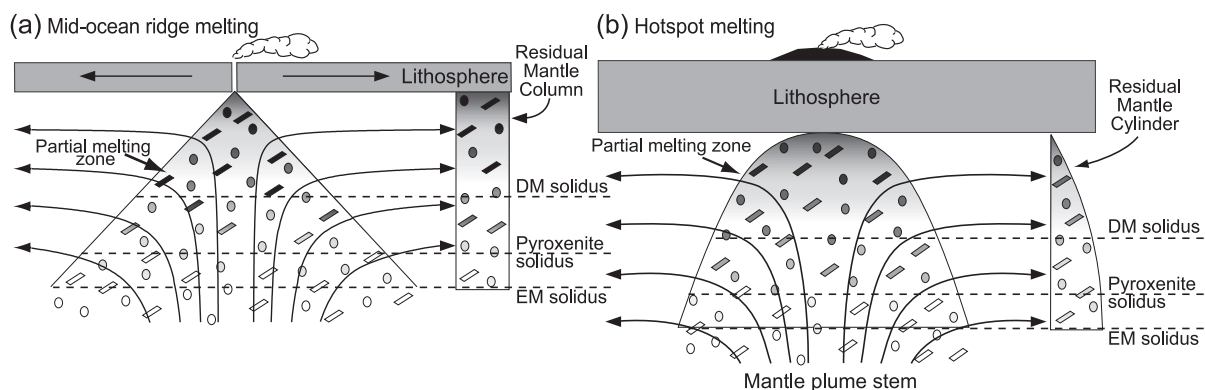


Fig. 1. Cartoons of mantle flow (streamlines) and melting of a heterogeneous mantle. Small blobs of enriched mantle (EM-ovals) and pyroxenite (prisms) are imbedded in a matrix of depleted mantle (DM). Shading of each material increases with increasing extent of partial melting. Incompatible trace elements enter the melt most abundantly near the solidi (dashed lines) of the respective lithologies. (a) Mantle flow beneath mid-ocean ridges driven passively by plate spreading generates a “residual mantle column” (RMC) nearly uniform in width. (b) Mantle plume flow beneath rigid plate generates a “residual mantle cylinder” (RMC) that widens with depth. Relative to mid-ocean ridges, mantle plumes tend to sample proportionally more EM and PX if they rise beneath thicker lithosphere and because of the more rapid plume flow (i.e., wider RMC) near the base of the melting zone.

derived more substantially from the EM and PX sources. This is one reason our model predicts plume melting to sample EM and PX materials proportionally more than mid-ocean ridge melting. Another factor is lithospheric thickness. Ocean islands can erupt on old seafloor where the lithosphere can be thicker than at mid-ocean ridges. Thicker lithosphere tends to limit the overall extent of partial melting as well as the amount of DM melting. While plume flow and thick lithosphere tend to reduce the relative amount of DM contributing to the melt, the one factor that tends to enhance the DM contribution is elevated temperature. Elevated temperatures of mantle plumes increase the extent of partial melting of all lithologies, including DM.

4. Global systematics

4.1. Variations with seafloor age

As lithospheric thickness is likely to limit the amount to which the mantle decompresses and melts, Ito and Mahoney [1] examined La/Sm and Sr, Nd, and Pb isotope ratios observed in OIBs vs. the age of the surrounding oceanic crust at the time of volcanism. Our models did reasonably well at predicting the general observations that OIBs erupting on older seafloor

(>~16 m.y.) display large geochemical variability, extending from compositions well within to well outside the MORB range, whereas OIBs erupting on younger seafloor show more limited overall variability, overlapping more substantially with the MORB compositions. The tendency for near-ridge hotspots to display compositions overlapping with those of many MORBs has been well documented (e.g., [19,58,59]). Some authors have proposed that the thin lithosphere near mid-ocean ridges enhances the ability of a predominantly DM-like ambient asthenosphere to dilute the predominantly EM- or PX-like material of an interacting mantle plume (e.g., [58,59]). We offer an alternative explanation: the more MORB-like compositions of the near-ridge hotspots arise out of a heterogeneous mantle that contains all components, but DM is more heavily expressed where melting is most extensive beneath thin near-ridge lithosphere. This notion has recently been proposed to explain the temporal change in composition of the Emperor seamounts [60] and compositions in Iceland [61]. We attribute the larger compositional variability of intraplate hotspots to a greater sensitivity of relatively low-degree partial melts to differences in mantle temperature and source composition. In addition, greater variability at intraplate hotspots can be expected as a direct consequence of a low overall volume of mantle melting at such hotspots compared to mid-ocean ridges

[49]. Potential causes for geochemical variations along hotspot-influenced ridges are discussed in Section 6.4.

4.2. Incompatible trace element patterns

The differences in mantle flow and melting conditions between hotspots and mid-ocean ridges can also account for characteristic differences in many trace elements between OIBs and MORBs, as illustrated in Fig. 2. Models that simulate mid-ocean ridge conditions of uniform $U(z)$, normal mantle temperatures (1350 °C), and thin lithosphere (7 km in thickness) predict relatively flat incompatible-element patterns that lie within the range for MORB. The mean pattern for MORB is itself relatively flat as we include “E-(enriched) type” MORB together with what most geochemists consider “N-(normal) type”, or “depleted” MORB. Model concentrations fall near the observed median values within the characteristic scatter, defined as one standard deviation of the natural log of the MORB compositions. The predicted compositional range is smaller than the characteristic scatter of the MORB data and much smaller than the total MORB range for each element shown. As

discussed by Ito and Mahoney [1], the models simulate perfect mixing of all melts generated. In reality, incomplete mixing of melts from different parts of the melting zone would naturally cause a wider range in compositions.

We also show examples of predictions for plume conditions of melting in which $U(z)$ increases with depth, average potential temperature is elevated (in this case, $T=1450$ °C), and the lithosphere is thick (in this case, the thickness is 80 km). These predictions span a broader total range (with changes in ϕ_{EM}/ϕ_{PX}) and extend to compositions that are more enriched in the highly incompatible elements, much like the OIB data.

4.3. Correlation between isotope and trace element ratios

Our models simulate perfect mixing between all melts generated from the base of the melting zone to a specified minimum depth (or maximum extent of partial melting). Thus, if individual lavas or magma batches (commonly represented by data for a single sample) represent mixtures of such aggregated melts, the models can be used to explore causes for

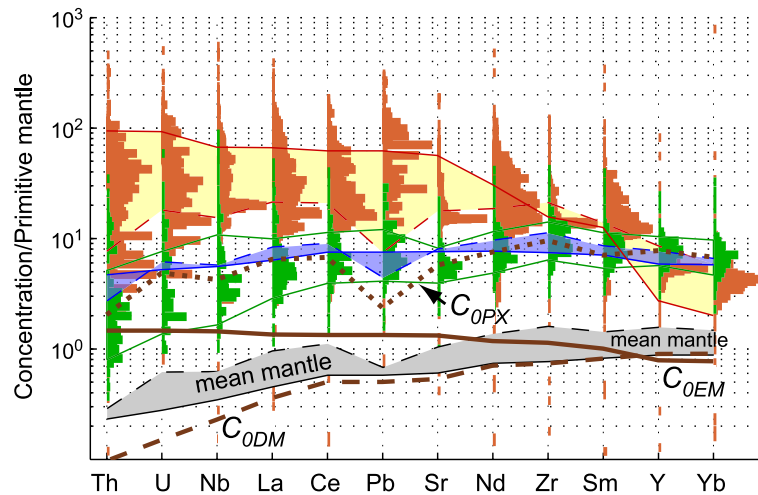


Fig. 2. Trace element patterns predicted for model mid-ocean ridges (blue) and intraplate hotspots under 64-M.y.-old lithosphere (yellow) are compared with data for MORBs (green) and OIBs (orange), displayed as histograms. Green lines mark one standard deviation of the natural log of the MORB data about the MORB median values. Concentrations are normalized by estimates for primitive mantle [71]. Calculations assume mass fraction of DM, EM, and PX in the mantle of $\phi_{DM}|\phi_{EM}|\phi_{PX}=0.9|0.1|0.0$ (blue and red solid) and $0.9|0.0|0.1$ (blue and red dashed). Heavy brown lines show assumed source compositions for DM (C_{ODM} , dashed), EM (C_{OEM} , solid), and pyroxenite (C_{OPX} , dashed-dotted). Weighted by their respective mantle fractions, these compositions yield average mantle compositions for $\phi_{DM}|\phi_{EM}|\phi_{PX}=0.9|0.1|0.0$ (solid black line) and $\phi_{DM}|\phi_{EM}|\phi_{PX}=0.9|0.0|0.1$ (dashed black line); gray mean mantle field is produced by varying the proportion of PX and EM between these compositions.

covariations between different geochemical ratios. Examples of such covariations are the “mantle arrays” in Nd–Sr–Pb isotope space defined by compositions within individual hotspots (e.g., [5,18,62]). We addressed these isotopic arrays in [1] and will revisit them in further detail in a later section, but first, we address observed correlations between trace element and isotope ratios.

General features of our global data set include overall tendencies of $^{87}\text{Sr}/^{86}\text{Sr}$ to increase and

$^{143}\text{Nd}/^{144}\text{Nd}$ to decrease with increasing La/Sm (Fig. 3). In contrast, $^{206}\text{Pb}/^{204}\text{Pb}$ both increases and decreases with increasing La/Sm; whereas $^{208}\text{Pb}/^{204}\text{Pb}$ generally increases for La/Sm=0.7–3.5 but does not show an obvious change for La/Sm>3.5. In all cases, the variability in isotope composition is minimal at low La/Sm (near most MORB values) and tends to increase with La/Sm (away from most MORB).

These characteristics are broadly predicted by the examples of plume calculations (Fig. 3). Models

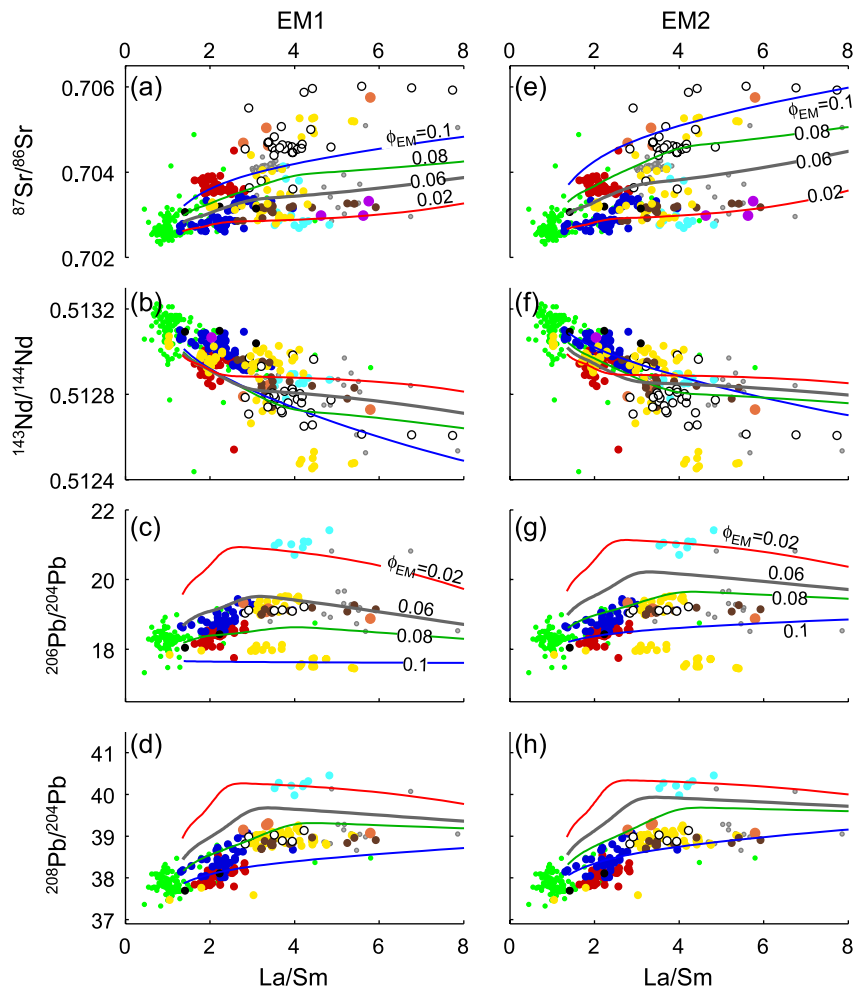


Fig. 3. Observed and predicted (lines) correlations between isotope ratios and La/Sm. Data for some hotspots are gray; others are colored: Iceland (black) Galápagos (dark blue), Easter (purple), Pitcairn (yellow), Cook-Austral (light blue), Hawaii and Hawaiian-Emperors (red), Society (white), Canary (brown), Samoa (orange). Green circles show normal MORB data. Calculations are for mantle plume flow in which excess mantle temperature is $\Delta T=100^\circ\text{C}$. Initial fraction of DM in the mantle is $\phi_{\text{DM}}=0.9$; numbers indicate fraction of EM in the starting mantle, with PX composing the remaining portion. EM is isotopically similar to the postulated “EM 1” end-member in panels (a)–(d) and similar to the postulated “EM 2” in panels (e)–(h).

predict low La/Sm to occur when DM is melting substantially and higher La/Sm when EM and PX are dominantly melting. Consequently, models successfully predict the general trends and increasing total variability of the observed $^{87}\text{Sr}/^{86}\text{Sr}$ and $^{143}\text{Nd}/^{144}\text{Nd}$ with increasing La/Sm. Predicted variations in Pb isotopes are slightly more complex owing to the highly radiogenic Pb assumed for PX and much less radiogenic Pb assumed for EM. When only a small amount of PX is present (e.g., $\phi_{\text{PX}}=0-0.02$; $\phi_{\text{EM}}=0.1-0.08$), models predict minimal increases or even small decreases in $^{206}\text{Pb}/^{204}\text{Pb}$ and $^{208}\text{Pb}/^{204}\text{Pb}$ with increasing La/Sm. With larger amounts of PX, $^{206}\text{Pb}/^{204}\text{Pb}$ and $^{208}\text{Pb}/^{204}\text{Pb}$ are predicted to first rise sharply for La/Sm=1–3 and then decrease gradually at higher La/Sm.

The predicted trends also show consistencies with trends of individual island groups such as Galápagos, Canary, Samoa, and to a lesser degree, Easter, Iceland, Cook-Austral, and Society. The Pitcairn data plot in two groups: a group (Pitcairn island) with higher $^{87}\text{Sr}/^{86}\text{Sr}$ (≥ 0.7035) and lower $^{143}\text{Nd}/^{144}\text{Nd}$ (≤ 0.5128) and $^{206}\text{Pb}/^{204}\text{Pb}$ (< 18.5) [63,64]; and a group (volcanoes northwest of Pitcairn) with lower $^{87}\text{Sr}/^{86}\text{Sr}$ and higher $^{143}\text{Nd}/^{144}\text{Nd}$ and $^{206}\text{Pb}/^{204}\text{Pb}$. The two groups likely reflect melting of distinct sources [65], but each group individually show trends with La/Sm that are broadly similar to those predicted by the models. Correlations between these isotope ratios, La/Sm, and other incompatible element ratios found in lavas from the EPR also support the concept of variable melt extraction from a heterogeneous mantle beneath mid-ocean ridges discussed by Niu et al. (e.g., [29,66]).

Having emphasized the consistencies between model calculations and observations, we also note that there are some cases in which model predictions oppose observations. One example is the Hawaiian islands, in which lavas with stronger EM-type isotope signatures (e.g., Koolau shield) tend to be relatively depleted in highly incompatible elements, and lavas with more DM-like isotopic signatures (e.g., Kilauea) show relative enrichments in the most incompatible elements [27,67]. This is also true for comparisons between shield lavas and rejuvenated-stage lavas [68,69]. For the Galápagos islands, weak negative correlations or at least a lack of positive correlations are evident between incompatible elements such as Na and $^{87}\text{Sr}/^{86}\text{Sr}$ [20]. Overall, a straightforward interpretation is that the EM-like source material is melting

more extensively than the material with the more DM-like isotopic characteristics. Indeed, our models always predict EM to melt more extensively than DM, but because we assume melts always mix in proportion to their rate of production, we cannot predict the observed relationships. This is an important limitation of our current method.

The model calculations shown in Figs. 2 and 3 are not meant to be comprehensive and are subject to a variety of simplifying assumptions, including those associated with our treatment of fractional melting, evolution of the solid phases, melt-solid partition coefficients, not to mention the uniform compositions of each lithology. Nevertheless, these sample calculations demonstrate how the melting process alone can explain many basic geochemical trends and compositional diversity in the OIB and MORB data.

5. Testing for a nonlayered mantle: optimal OIB mantle sources and predicted MORBs

We now test for the possibility of a nonlayered heterogeneous mantle by first optimizing calculations to fit isotope trends of several individual hotspot island groups. The successful models identify the possible starting mantle compositions that can explain the observations when plume conditions of melting are applied. We then “melt” these same mantle compositions under normal mid-ocean ridge conditions and compare predicted MORB compositions with the observed MORB composition. If the predictions are characteristically different from observed MORB compositions, then a distinction between the OIB and MORB sources would be implied. This result would be compatible with a layered mantle, assuming mantle plumes deliver deep mantle material to hotspots. Alternatively, if the OIB sources predicted MORB compositions indistinguishable from the observations, then there would be no need for a distinction between OIB and MORB sources and, by extension, for a layered mantle.

5.1. Method

The approach we take is a grid search through parameter space to fit the isotope trends observed at individual hotspots. We seek solutions for five inde-

pendent variables. The first variable is average mantle temperature excess (relative to 1350 °C), and we consider values of $\Delta T=50, 100, \text{ and } 200$ °C. The next two variables are the mass fractions of each lithology in the starting mantle: the mass fraction ϕ_{DM} of DM is varied between 0.2 and 0.95 in increments of 0.05, and the mass fraction ϕ_{EM} of EM is varied between 0.0 and 0.1 in increments of 0.0125, and $\phi_{PX}=1-\phi_{DM}-\phi_{EM}$. The concentrations of Sr, Nd, and Pb assumed for each lithology are those shown in Fig. 2.

The last two variables are the isotopic compositions of the EM and PX lithologies. They are assumed to be inherent mixtures of three out of four global end-member components [18]. The isotope composition of EM, for example, is explored using the following methodology. If I_{EM} is an arbitrary isotope ratio for EM,

$$I_{EM} = f_{EM}I_{EM0} + f_{DM}I_{DM0} + (1 - f_{DM} - f_{EM})I_{PX0}. \quad (1)$$

Here, the ratios in the global end-member component I_{DM0} , I_{PX0} , I_{EM0} are similar to DMM, HIMU, and EM1

or EM2 [18], respectively. Variables f_{DM} and f_{EM} are isotopic mixing fractions. Inversions search values of f_{EM} in seven increments of 0.1 over the range 0.4–1 (Fig. 4). The remaining mixing fraction ($1-f_{EM}=0.6-0$) is then a variable mixture of the DM and the PX (i.e., $f_{DM}=(1-f_{EM})f$, with f in 11 increments 0.1 over the range 0–1). The search increments of f_{EM} and f define ($7 \times 11=77$ points in the four-isotope-ratio ($^{87}\text{Sr}/^{86}\text{Sr}$, $^{143}\text{Nd}/^{144}\text{Nd}$, $^{206}\text{Pb}/^{204}\text{Pb}$, and $^{208}\text{Pb}/^{204}\text{Pb}$) space. To “fill in” the volume between these points, we consider the EM source to span a small range about I_{EM} (filled EM triangle in Fig. 4). We are essentially assuming EM itself is heterogeneous, spanning a limited range of compositions about I_{EM} . This inherent heterogeneity gives a compositional “width” to a predicted isotope array for fitting to the observed arrays.

The isotope composition of the PX lithology is computed in an analogous fashion. Making I_{PX0} similar to HIMU is a convenient way to ensure that the inversions search through a full range of Sr–Nd–Pb isotope space. However, as few OIB compositions actually approach HIMU, many of our solutions for I_{PX} and occasionally I_{EM} , instead, end up being more

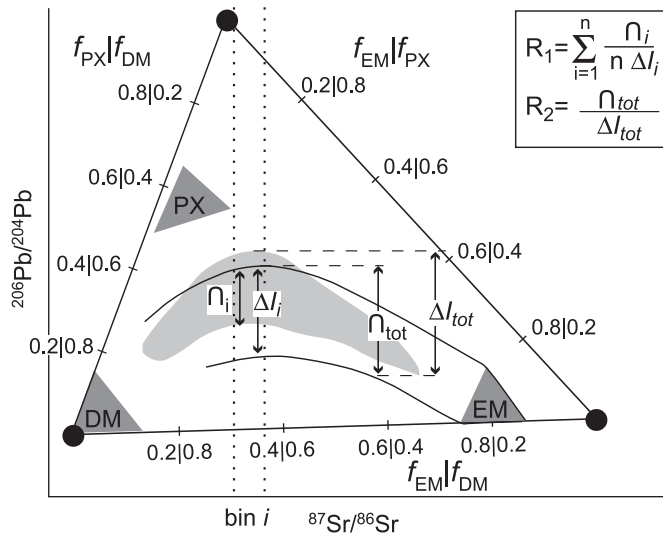


Fig. 4. Illustration of the method used to define the isotope compositions of the mantle lithologies and fitting parameters R_1 and R_2 . Mantle lithologies (marked DM, EM, PX) are themselves heterogeneous, spanning the compositions shown by the dark triangles. The positions of these triangles are specified by ternary mixtures of the assumed compositional end-member components (dots). Edges of the trial compositional space are marked according to the mixing fractions (f_{DM}, f_{EM}, f_{PX}) of the end-member components. In this case, the dependent variable for fitting is $^{206}\text{Pb}/^{204}\text{Pb}$, and the independent variable is $^{87}\text{Sr}/^{86}\text{Sr}$. Gray field represents data; solid curves bound the range of model values. Dotted lines mark the Sr isotope bin in which the model range ΔI_i and the overlap between model and data \cap_i are computed. The mean normalized overlap is R_1 , and the total normalized overlap is R_2 .

similar to the common “C” or “FOZO” end-member component [8,18] (unlike what we did originally in [1]). In this way, we incorporate the Sr–Nd–Pb isotopic composition of C or FOZO (the noble gas composition of this end-member is discussed in Section 6.2). For DM, we assume only one value of I_{DM} , near the value of the DMM global end-member component.

For each set of parameter values (i.e., trial solution), we compute magma compositions by integrating over increasing heights of the melting zone, beginning at the base of the melting zone and ending at the base of the lithosphere, the depth of which is a function of the square-root of the age of seafloor on which the OIB erupted. For each hotspot, we fit seven isotope correlations: $^{206}\text{Pb}/^{204}\text{Pb}$ (on the ordinate it is the dependent variable, see Fig. 4) as a function of $^{87}\text{Sr}/^{86}\text{Sr}$, $^{143}\text{Nd}/^{144}\text{Nd}$, and $^{208}\text{Pb}/^{204}\text{Pb}$

(on the abscissa, each is the independent variable), and the four isotope ratios (dependent variables) as a function of seafloor age at the time of volcanism (independent variable).

The wide scatter of the observed compositions, particularly as a function of seafloor age, prohibits standard fitting techniques; therefore, we devise an ad hoc method of fitting, based on two fitting parameters. The first parameter is computed by dividing the independent variable (e.g., $^{87}\text{Sr}/^{86}\text{Sr}$ in Fig. 4) into discrete bins. For a given bin (i), we compute the amount of overlap (\cap_i) in the dependent variable (e.g., $^{206}\text{Pb}/^{204}\text{Pb}$) between the model predictions and the data. This overlap is normalized by the model compositional range (ΔI_i) and then averaged. This average is the fitting parameter R_1 (see Fig. 4). High values of R_1 ensure that model solutions overlap with the observed trends but extend minimally outside of

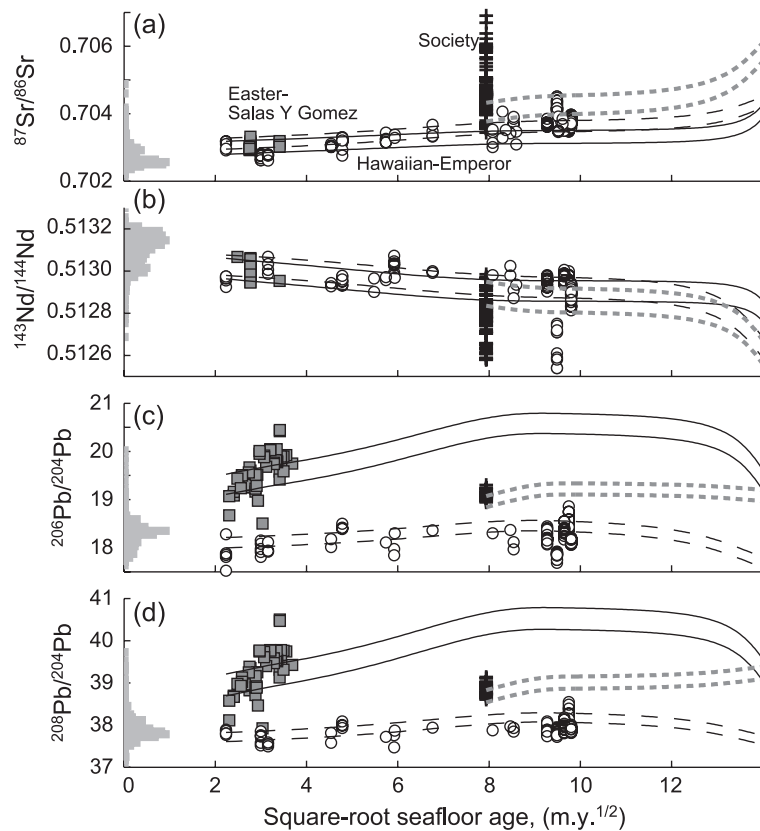


Fig. 5. Examples of model predictions compared with observations for the Easter-Salas y Gomez chain (solid curves and gray squares, respectively), Hawaii and the Hawaiian-Emperors (long dashed curves and white circles), and Society chains (short dashed curves and plus signs). MORB data are shown as gray histograms on the vertical axis.

the observed compositional range within each bin of the independent variable. The second parameter R_2 is calculated by measuring the overlap between the full isotope range of the hotspot data set and the total range predicted by the model \cap_{tot} . Normalizing \cap_{tot} by the total span of the observed isotope ΔI_{tot} yields R_2 . High values of R_2 ensure that models predict appreciable lengths of the observed isotope arrays.

For a given model calculation, R_1 and R_2 are computed for each isotope. We consider the solution acceptable if the minimum R_1 and the minimum R_2 exceed specified values: $R_1 \geq 0.2$ and $R_2 \geq 0.5$. Basing our fitting criteria on the minima of R_1 and R_2 guarantees a minimum fit for all isotope ratios considered. Average values of R_1 and R_2 for acceptable solutions typically exceed 0.6 and 0.7, respectively. The grid search performed for each hotspot involved testing as many as 390,000 possible combinations of the five variables (ϕ_{DM} , ϕ_{EM} , I_{PX} , I_{EM} , and ΔT).

5.2. Fitting hotspot isotope trajectories

Here we discuss some examples of our model fits. For the most part, the island groups for which we have sufficient data have erupted on seafloor having only a very limited range of age within any given group. Lavas along the Hawaiian and Hawaiian-Emperor chains are an exception, having been emplaced on seafloor ages from <10 m.y. (Meiji and Detroit seamounts [70]) to ~95 m.y. (Kilauea). This range of seafloor ages provides an ideal opportunity to first test the predicted effects of lithospheric thickness and then to constrain the source compositions that could have generated these magmas.

Fig. 5 illustrates an example solution, which fits the Sr, Nd, and Pb isotope data for the Hawaiian hotspot chain as a function of seafloor age. Model predictions overlap reasonably well with the observations over the full range of seafloor ages; they match the decrease in $^{206}\text{Pb}/^{204}\text{Pb}$ and $^{87}\text{Sr}/^{86}\text{Sr}$, and increase in $^{143}\text{Nd}/^{144}\text{Nd}$ with decreasing seafloor age. However, as the predicted compositional range at a single seafloor age is limited by the inherent heterogeneity of each source lithology, the model is unable to predict the large diversity in the data for the Hawaiian islands, as is most evident in $^{143}\text{Nd}/^{144}\text{Nd}$ (Fig. 5b). Models can only explain this large diversity, again, if the lava

samples represent incomplete mixtures of magmas generated at different depths in the melting zone. Figs. 6a–c illustrate that the model indeed fits the Hawaiian island data in isotope–isotope space, including the bends or cusps in the trajectories of $^{87}\text{Sr}/^{86}\text{Sr}$ (near 0.7035) vs. $^{206}\text{Pb}/^{204}\text{Pb}$, $^{143}\text{Nd}/^{144}\text{Nd}$ (near 0.5129) vs. $^{206}\text{Pb}/^{204}\text{Pb}$, and $^{208}\text{Pb}/^{204}\text{Pb}$ vs. $^{206}\text{Pb}/^{204}\text{Pb}$ (near 18.5). Deep melting is predicted to produce the mixing branch between the EM and PX compositions, which follow the data for the Hawaiian islands, whereas shallower (DM) melting is predicted to bend the trajectory toward the composition of DM, following the data for the Hawaiian-Emperor volcanoes. For reference, the minimum value of R_1 is 0.34, and the minimum R_2 is 0.8. The mantle source for this calculation has $\phi_{\text{DM}}|\phi_{\text{EM}}|\phi_{\text{PX}}=0.9|0.05|0.05$ (the isotopic compositions of each lithology shown by the triangles in Fig. 6) and $\Delta T=100$ °C. This combination of successful input parameters is one of ~15,000 other combinations that produced acceptable fits. Our results support the proposal of [60] that the isotopic compositions of the Hawaiian-Emperor seamounts reflect melting beneath a thinner lithosphere which allows more extensive DM melting.

Data for the Easter-Salas y Gomez hotspot span a more limited range of seafloor age (2–15 m.y.; Fig. 5). Models successfully overlap with the data and predict a trend toward MORB compositions with decreasing seafloor age. The observed slopes of the Pb isotope ratios vs. age, however, appear to be greater than predicted (Fig. 5). One possible explanation for this discrepancy is that there is a change in the composition of the source from the Easter-Salas y Gomez hotspot toward the EPR [52], which our models do not include. Alternatively, there could be a westward change in the style of mantle flow, with plume flow beneath the hotspot, which tends to enhance PX signatures, and mid-ocean ridge flow near the EPR, which tends to enhance the DM signatures. The solution summarized in Fig. 6 also predicts the observed compositions in isotope space, although the Nd and Sr data are few in number. The minima of R_1 and R_2 are 0.21 and 0.91, respectively, $\Delta T=100$ °C, and the source has $\phi_{\text{DM}}|\phi_{\text{EM}}|\phi_{\text{PX}}=0.9|0.013|0.087$. This is one of 7200 acceptable solutions.

Lastly, we show fits to data for the Society hotspot. In this case, there is no resolvable variation in seafloor age at the time of volcanism, despite a particularly

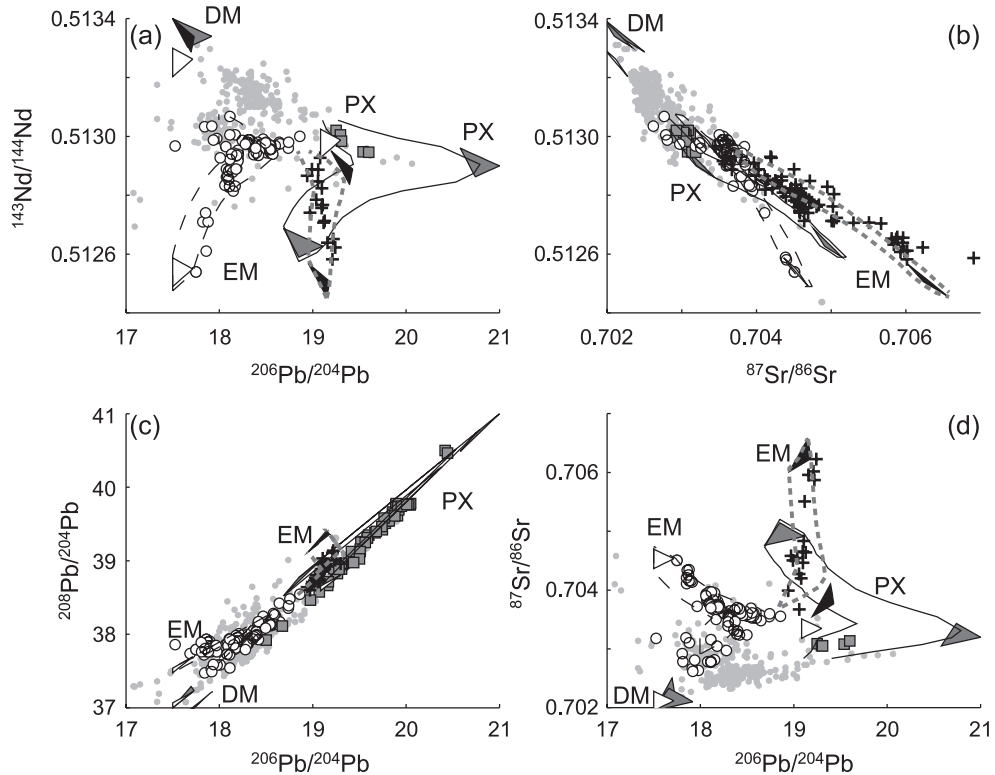


Fig. 6. Examples of models that fit the observed isotope arrays for the same three hotspots (and same symbols and curves) as in Fig. 5. Large triangles (gray for Easter-Salas y Gomez, white for Hawaii and the Hawaiian-Emperor chain, and black for Society) show the inherent compositional range of each model lithology.

wide range in Sr and Nd isotopic compositions (Fig. 5). Model compositions can therefore overlap with only a small portion of the Society data. In isotope space, however, models successfully predict the $^{87}\text{Sr}/^{86}\text{Sr}$ and $^{143}\text{Nd}/^{144}\text{Nd}$ variations vs. each other and vs. the Pb isotope ratios (Fig. 6). This calculation fits the observations with a minimum $R_1=0.29$ and minimum $R_2=0.79$, $\Delta T=100$ °C, and the source has $\phi_{\text{DM}}|\phi_{\text{EM}}|\phi_{\text{PX}}=0.02|0.95|0.03$. It is one of 30,700 other model solutions that fit the Society data to within our specified tolerance.

5.3. Predicted MORB compositions from successful OIB mantle sources

We have shown three examples of models that produced acceptable fits to data for three hotspots. The solutions identify specific mantle compositions, defined by the relative fractions (ϕ_{DM} , ϕ_{EM} , ϕ_{PX})

and the isotopic compositions (I_{DM} , I_{EM} , I_{PX}) of each lithology. We now examine the MORB compositions that all successful sources for these and 10 other hotspots would produce if the sources melted beneath a mid-ocean ridge. The mid-ocean ridge conditions we assume are a lithospheric thickness of 7 km, a normal mantle potential temperature of 1350 °C, and uniform flow out of the melting zone ($U(z)$ is constant).

Figs. 7a–d summarize predicted MORB compositions from all of the successful OIB sources, which represent the full range of ϕ_{DM} tested (0.2–0.95). The results are shown as histograms; the length of each bar is proportional to the number of successful solutions in that compositional bin and is thus proportional to the volume spanned by that set of solutions in four-dimensional (ϕ_{DM} , ϕ_{EM} , I_{EM} , I_{PX}) source composition space. The histograms can be viewed as probability functions to the extent that the likelihood of a given MORB composition is proportional to the

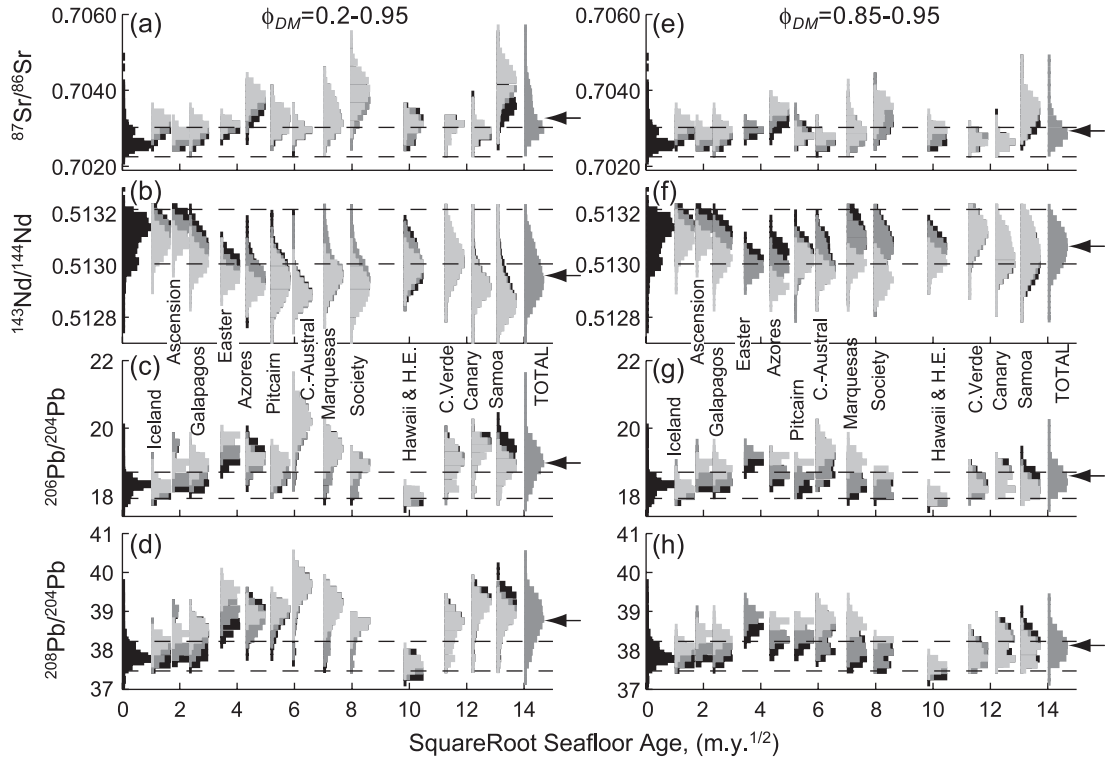


Fig. 7. (a–d) All mantle sources (range of tested fraction DM in source, ϕ_{DM} , is indicated at top) that fit the data for the labeled hotspots (Pitcairn and Samoa values are shifted to the right by 1 m.y. for clarity) are melted under mid-ocean ridge conditions (see text) to produce the predicted MORB compositions shown. Results are displayed as histograms on the vertical axis, indicating the number of solutions that fall within the indicated compositional bins. For the hotspots, black, dark gray, and light gray correspond to solutions that fit the hotspot data with mean mantle temperature anomalies of $\Delta T=50$, 100, and 200 °C, respectively. Dark gray histograms at seafloor age of 14 m.y.^{1/2} show the cumulative numbers for all the hotspot models, with median compositions marked by arrows. Black histograms at 0 m.y.^{1/2} are for MORB data (same as in Fig. 5), with one standard deviation away from the median marked by dashed lines. (e–h) Same as in the left column but only for models with mantle sources mostly composed of DM (source fraction DM is $\phi_{DM}=0.85-0.95$). On average, PX is slightly more abundant than EM; that is, for $\phi_{DM}=0.85-0.95$, the average of ϕ_{PX}/ϕ_{EM} is 1.17, and for $\phi_{DM}=0.20-0.95$, the average of ϕ_{PX}/ϕ_{EM} is 1.44.

volume spanned in composition space. The observed MORB range is defined as one standard deviation away from the median of the MORB data. Most of the predicted compositions lie outside of the observed MORB range. This result illustrates what is already understood: it is straightforward to explain OIB compositions with sources that are distinct from the MORB source.

Figs. 7e–h show histograms of the subset of solutions restricted to mantle sources containing $\geq 85\%$ DM ($\phi_{DM}=0.85-0.95$). Intuitively, larger fractions of DM result in more DM-like MORB compositions. Some of the OIB sources yield predicted compositions that are outside of the defined MORB range, but the sources for Ascension, Canaries, Cape

Verde, Galápagos, Hawaii, Iceland, and Marquesas yield median MORB compositions (or $>50\%$ of the solutions) within the observed MORB range for all four isotope ratios. The sources for these hotspots are thus most likely to be indistinguishable from the mantle that commonly melts beneath mid-ocean ridges. For Samoa, median compositions for $^{87}\text{Sr}/^{86}\text{Sr}$ are slightly greater than that of the observed MORB range, but $>50\%$ of the predicted compositions fall within the MORB range for all of the other isotope ratios. For Pitcairn, median compositions fall within the MORB range for all isotopes but $^{208}\text{Pb}/^{204}\text{Pb}$. Easter-Salas y Gomez and Cook-Austral sources yield median $^{87}\text{Sr}/^{86}\text{Sr}$ and $^{143}\text{Nd}/^{144}\text{Nd}$ compositions within the MORB range and median $^{206}\text{Pb}/^{204}\text{Pb}$ and

$^{208}\text{Pb}/^{204}\text{Pb}$ compositions outside of the MORB range; Azores sources yield median $^{143}\text{Nd}/^{144}\text{Nd}$ and $^{206}\text{Pb}/^{204}\text{Pb}$ compositions within the MORB range and median $^{87}\text{Sr}/^{86}\text{Sr}$ and $^{208}\text{Pb}/^{204}\text{Pb}$ outside the MORB range. The sources of Easter-Salas y Gomez, Cook-Austral, and Azores groups are thus most likely to be distinct from the mantle commonly melting beneath mid-ocean ridges. Finally, when the solutions for all of the hotspots are combined, we see that the median solutions fall within the MORB range for all isotopes. Thus, >50% of the hotspot sources that fit the OIB data produce theoretical compositions that are not distinguishable from the actual MORB compositions. The results of this exercise suggest that although geographic variations in mantle compositions of Sr, Nd, and Pb isotopes are required, global geochemical layering in the portion of the mantle that produces OIB and MORB volcanism may not be required.

6. Discussion: possibility of a nonlayered heterogeneous mantle

6.1. Incompatible trace element and heat budget

For those models that yield indistinguishable MORB and OIB compositions, it is necessary to evaluate whether the implied mean mantle composition can represent that of the entire mantle. With few exceptions, the incompatible trace element contents of the bulk continental crust and the present-day mantle should sum approximately to those of the primitive mantle. If we assume, for reference, that the whole mantle is 90% DM and the remaining 10% is a mixture of EM and PX, the compositions assumed for these lithologies yield the bulk mantle compositions shown by the gray field in Fig. 2. This predicted present-day mantle would contain 25–30% and 30–60% of the primitive mantle content [71] of Th and U, respectively. Estimated ranges for the continental crust are 25–60% for Th and 25–50% for U (see [72] and references therein). The lower-bound percentages of our model mantle, combined with the continental estimates, would imply the presence of a “hidden” reservoir containing the remaining portion of these elements but suggest that this reservoir is smaller than previously postulated [43]. On the other hand, our

upper-bound model values combined with the upper-bound continental estimates would minimize or do away with the need for this additional reservoir.

Another consideration is the Earth’s heat budget. If continents generate 6–7 TW [73] of the Earth’s total heat loss of ~44 TW [74], then the remaining 37–38 TW from the mantle and core is in part primordial and in part generated by radioactivity of the major heat-producing elements U, Th, and K. Our model mantle composition would produce roughly 30–60% of the ~20 TW [73] of radioactive heat that primitive mantle would presently generate; thus, if our mantle composition represents that of the whole mantle, <~30% of the mantle and core’s heat must be radiogenic. This percentage is small, but it can allow for reasonably low secular cooling rates if the retardation of global heat loss by a thick compositional lithosphere (formed by partial melting) is important [2]. We conclude that, on the basis of these arguments, the possibility of a nonlayered mantle with a mean composition similar to that of our models cannot presently be rejected.

6.2. FOZO and C and the undegassed source

One argument for a distinct lower-mantle source for OIBs (and by inference, plumes) is that the Nd–Sr–Pb isotopic arrays for several widely separated ocean island groups suggest the involvement of a common global end-member component that is different from DM [18]. Although our models address this component in Nd–Sr–Pb isotope space, what may be more telling are the noble gas compositions. In particular, this end-member (termed “FOZO” or “C”) is associated with higher $^3\text{He}/^4\text{He}$ than estimated for DM [8]. To most workers, the He isotope data suggest a reservoir that has experienced comparatively little degassing of primordial He (^3He). Such material is usually argued to be in a convectively isolated lower mantle, which is sampled by deep-seated mantle plumes but is largely secluded from mid-ocean ridge melting. However, the long-term preservation of undegassed material does not necessarily require mantle layering. That a non-layered mantle will retain an appreciable amount of relatively undegassed material is implied by the estimated ~5 G.y. needed to process the whole mantle by mid-ocean ridge melting [23] and is predicted by models of mantle convection that match present-day

plate motions and surface heat flow [37]. Indeed, evidence for the global presence of the high $^3\text{He}/^4\text{He}$ component in both MORBs and OIBs [8] supports this possibility. Like the other isotope end-members, our models would predict OIBs to more heavily sample this high ^3He material if it begins melting deeper than DM. We propose that rather than reflecting stratification in the locations of mantle components, the observed isotopic mixing arrays instead reflect stratification in the melting of the different components. The growing noble gas [75] data set should allow for various tests of the this hypothesis.

6.3. *Ultraslow spreading centers*

We have emphasized the importance of lithospheric thickness on magma composition. Another test for a nonlayered heterogeneous mantle would be to examine MORB compositions at ridges with unusually thick lithosphere, such as ultraslow spreading ridges. Available samples from ultraslow-spreading sections of the Southwest Indian [25,76] and the Gakkel ridges [77] tend to have elevated abundances of incompatible elements compared to more typical MORB compositions. These observations, in addition to unusually thin or even absent crust, suggest unusually low average extents of partial melting, as is expected for melting beneath thick lithosphere. Southwest Indian Ridge MORBs also show unusually large variations in Nd isotopes [55] as well as correlations between Nd isotopes and La/Sm [78]. These observations have been explained by a veined mantle (e.g., [25]), but whether the compositions of this mantle can be representative of the whole mantle is yet to be explored.

6.4. *Geographic variations at hotspots*

Another argument for a geochemical distinction between the sources of mantle plumes and MORBs comes from correlated physical and geochemical anomalies at ridges interacting with hotspots (e.g., [4,79]). We suggest the alternative possibility that the geochemical anomalies do not reflect source variability but instead arise from the process of melting and melt extraction. We have demonstrated that thick lithosphere and plume-driven mantle flow can enhance the expressions of PX and EM in melts, relative to thin

lithosphere and normal mid-ocean ridge mantle flow. However, mantle plumes are also likely to be hotter than nonplume mantle and therefore melt DM more extensively. Ito and Mahoney [1] showed some examples of calculations in which the effects of lithospheric thickness and plume flow can overcome the effects of elevated temperature. These calculations were able to account for a large fraction of the variation between median Sr, Nd, and Pb isotope compositions of the ridge-centered Iceland hotspot and median compositions of normal sections of the MAR.

The models, however, fell well short of explaining the total variability at Iceland and along the MAR. An obvious shortcoming of the current methodology is that it simulates mixing of melts laterally from all portions of the melting zone. It therefore does not explore geochemical variability as a function of geographic position across an upwelling mantle plume or a plume interacting with a mid-ocean ridge. Moreover, the current models assume a plume of uniform (average) viscosity and temperature, whereas strong variations in both properties are likely to exist in the melting zone [80]. These effects could be explored with three-dimensional numerical models. Such models could also explore possible causes for geographic variations in magma chemistry at intra-plate hotspots, such as those documented around Hawaii [13,27,81].

6.5. *Constraints from major elements*

Finally, the current models only address incompatible trace element and isotope compositions. As major elements provide crucial information about pressures and extents of partial melting, they must be incorporated in future efforts to test and better constrain the scenario for a nonlayered mantle that we are proposing. An important challenge will be to understand how different lithologies in a veined mantle melt and how the chemistry of the melts from each lithology might change as the melts interact with each other and with the solid.

7. Conclusions

We conclude that a rich diversity of geochemical characteristics can arise by melting a heterogeneous

mantle under different conditions of lithospheric thickness, mantle flow, and temperature. Such differences can account for characteristic isotopic and incompatible trace element distinctions between OIBs and normal MORBs without any difference in the respective mantle sources. Progressive melt extraction from different depths in the melting zone can explain many features in observed correlations among La/Sm and Sr, Nd, and Pb isotopes. Models demonstrate that the observed changes in Sr, Nd, and Pb isotope ratios along the Hawaiian-Emperor chain can largely be explained by melting a heterogeneous mantle under lithosphere of decreasing thickness. The models can also explain covariations among these isotopes along the whole Hawaiian hotspot chain.

To test the possibility of a nonlayered mantle, we solve for the mantle source compositions that, when melted at excess temperatures, under thick lithosphere and with mantle plume flow, can explain Sr, Nd, and Pb isotope compositions of 13 hotspots. These mantle sources are then melted at normal mantle temperature, with mid-ocean ridge mantle flow, and under thin lithosphere to predict MORB compositions. Some solutions fall outside the observed MORB range, but those solutions that are indistinguishable from observed MORB compositions allow for the possibility of a nonlayered mantle. The implied mean incompatible-element content of such a mantle is relatively low but falls within the allowable range required to satisfy the U, Th, and heat budgets of the mantle.

This study is simplistic and falls short of a complete test in many ways. Future efforts should consider noble gas constraints (and the common C or FOZO end-member), focus on geochemical data from ultraslow-spreading ridges, examine geographic variations at hotspots, including hotspots interacting with mid-ocean ridges, and incorporate major elements. All such studies will benefit from new laboratory and theoretical insights into how heterogeneous systems melt and how melts from distinct lithologies interact with each other and with solid phases prior to erupting.

Acknowledgements

We appreciate Marc Hirschmann's and Paula Smith's careful reviews of both this and our companion

manuscript [1]. This project was funded by NSF grant OCE02-21889.

Appendix A. Background data sets

Supplementary data associated with this article can be found, in the online version, at [10.1016/j.epsl.2004.10.034](https://doi.org/10.1016/j.epsl.2004.10.034).

References

- [1] G. Ito, J. Mahoney, Flow and melting of a heterogeneous mantle. 1: method and importance to the geochemistry of ocean island and mid-ocean ridge basalts, *Earth Planet. Sci. Lett.* DOI:10.1016/j.epsl.2004.10.035.
- [2] J. Korenaga, Energetics of mantle convection and the fate of fossil heat, *Geophys. Res. Lett.* 30 (8) (2003) 1437.
- [3] S.R. Hart, J.-G. Schilling, J.L. Powell, Basalts from Iceland and along the Reykjanes Ridge: Sr isotope geochemistry, *Nat., Phys. Sci.* 246 (1973) 104–107.
- [4] J.-G. Schilling, Iceland mantle plume: geochemical study of Reykjanes Ridge, *Nature* 242 (1973) 565–571.
- [5] W.M. White, Sources of oceanic basalts: radiogenic isotopic evidence, *Geology* 13 (1985) 115–118.
- [6] G.J. Wasserburg, D.J. DePaolo, Models of earth structure inferred from neodymium and strontium isotope abundances, *Natl. Acad. Sci. Proc.* 76 (1979) 3594–3598.
- [7] S.R. Hart, Heterogeneous mantle domains: signatures, genesis and mixing chronologies, *Earth Planet. Sci. Lett.* 90 (1988) 273–296.
- [8] B.B. Hanan, D.W. Graham, Lead and helium isotope evidence from oceanic basalts for a common deep source of mantle plumes, *Science* 272 (1996) 991–995.
- [9] A.W. Hofmann, Mantle geochemistry: the message from oceanic volcanism, *Nature* 385 (1997) 219–229.
- [10] A.W. Hofmann, W.M. White, Mantle plumes from ancient oceanic crust, *Earth Planet. Sci. Lett.* 57 (1982) 421–436.
- [11] B.L. Weaver, D.A. Wood, J. Tarney, J.-L. Joron, Role of subducted sediment in the genesis of ocean island basalts: geochemical evidence from South Atlantic Ocean Islands, *Geology* 14 (1986) 275–278.
- [12] B.L. Weaver, Trace-element evidence for the origin of oceanic island basalts, *Geology* 19 (1991) 123–126.
- [13] E.H. Hauri, J.C. Lassiter, D.J. DePaolo, Osmium isotope systematics of drilled lavas from Mauna Loa, Hawaii, *J. Geophys. Res.* 101 (1996) 11793–11806.
- [14] W.J. Morgan, Convection plumes in the lower mantle, *Nature* 230 (1971) 42–43.
- [15] C.J. Allégre, D.L. Turcotte, Geodynamic mixing in the mesosphere boundary layer and the origin of oceanic islands, *Geophys. Res. Lett.* 12 (1985) 207–210.
- [16] V. Courtillot, A. Davaille, J. Besse, J. Stock, Three distinct types of hotspots in the Earth's mantle, *Earth Planet. Sci. Lett.* 205 (2003) 295–308.

- [17] G.F. Davies, Mantle plumes, mantle stirring and hotspot chemistry, *Earth Planet. Sci. Lett.* 99 (1990) 94–109.
- [18] S.R. Hart, E.H. Hauri, L.A. Oschmann, J.A. Whitehead, Mantle plumes and entrainment: isotopic evidence, *Science* 256 (1992) 517–520.
- [19] E.H. Hauri, J.A. Whitehead, S.R. Hart, Fluid dynamics and geochemical aspects of entrainment in mantle plumes, *J. Geophys. Res.* 99 (1994) 24275–24300.
- [20] W.M. White, A.R. McBirney, R.A. Duncan, Petrology and geochemistry of the Galápagos Islands: portrait of a pathological mantle plume, *J. Geophys. Res.* 98 (1993) 19533–19563.
- [21] N.H. Sleep, Tapping of magmas from ubiquitous mantle heterogeneities: an alternative to mantle plumes? *J. Geophys. Res.* 89 (1984) 10029–10041.
- [22] G.F. Davies, Geophysical and isotopic constraints on mantle convection: an interim synthesis, *J. Geophys. Res.* 89 (1984) 6017–6040.
- [23] C.J. Allégre, D.L. Turcotte, Implications of the two-component marble-cake mantle, *Nature* 323 (1986) 123–127.
- [24] H.J.B. Dick, R.L. Fisher, W.B. Bryan, Mineralogic variability of the uppermost mantle along mid-ocean ridges, *Earth Planet. Sci. Lett.* 69 (1984) 88–106.
- [25] A.P. le Roex, H.J.B. Dick, A.J. Erlank, A.M. Reid, F.A. Frey, S. Hart, Geochemistry, mineralogy, and petrogenesis of lavas erupted along the Southwest Indian Ridge between the Bouvet Triple Junction and 11 degrees east, *J. Petrol.* 24 (1983) 267–318.
- [26] A.E. Saal, R.L. Rudnick, G.E. Ravizza, S.R. Hart, Re–Os isotope evidence for the composition, formation and age of the lower continental crust, *Nature* 393 (6680) (1998) 58–61.
- [27] F.A. Frey, J.M. Rhodes, Intershield differences among Hawaiian volcanoes: implications for source compositions, melting process and magma ascent paths, *Philos. Trans. R. Soc. Lond. Ser. A: Math. Phys. Sci.* 342 (1993) 121–136.
- [28] A. Meibom, N.H. Sleep, C.P. Chamberlain, R.G. Coleman, R. Frei, M.T. Hren, J.L. Wooden, Re–Os isotopic evidence for long-lived heterogeneity and equilibration processes in the Earth's upper mantle, *Nature* 419 (2002) 705–708.
- [29] Y. Niu, G. Waggoner, J.M. Sinton, J.J. Mahoney, Mantle source heterogeneity and melting processes beneath seafloor spreading centers: the East Pacific Rise 18°–19° S, *J. Geophys. Res.* 101 (1996) 27711–27733.
- [30] K.C. Creager, T.H. Jordan, Slab penetration into the lower mantle below the Mariana and other island arcs of the Northwest Pacific, *J. Geophys. Res.* 91 (1986) 3573–3589.
- [31] S.P. Grand, Mantle shear structure beneath the Americas and surrounding oceans, *J. Geophys. Res.* 99 (1994) 11591–11621.
- [32] R. van der Hilst, Evidence for deep mantle circulation from global tomography, *Nature* 386 (1997) 578–584.
- [33] Y. Fukao, S. Widiyantoro, M. Obayashi, Stagnant slabs in the upper and lower mantle transition region, *Rev. Geophys.* 39 (2001) 291–324.
- [34] Y. Ricard, M. Richards, C. Lithgow-Bertelloni, Y. LeStunff, A geodynamic model of mantle density heterogeneity, *J. Geophys. Res.* 98 (1993) 21195–21909.
- [35] M.A. Richards, D.C. Engebretson, Large-scale mantle convection and the history of subduction, *Nature* 355 (1992) 437–440.
- [36] P. van Keken, E. Hauri, C. Ballentine, Mantle mixing: the generation, preservation, and destruction of mantle heterogeneity, *Annu. Rev. Earth Planet. Sci.* 30 (2002) 493–525.
- [37] P.E. van Keken, C.J. Ballentine, Whole-mantle versus layered mantle convection and the role of a high viscosity lower mantle in terrestrial volatile evolution, *Earth Planet. Sci. Lett.* 156 (1998) 19–32.
- [38] L.H. Kellogg, Mixing in the mantle, *Annu. Rev. Earth Planet. Sci.* 20 (1992) 365–388.
- [39] S. Ferrachat, Y. Ricard, Mixing properties in the Earth's mantle: effects of viscosity stratification and of oceanic crust segregation, *Geochem. Geophys. Geosyst.* 2 (2001) (2000GC000092).
- [40] D. Hunt, L.H. Kellogg, Quantifying mixing and age variations of heterogeneities and models of mantle convection: role of depth-dependent viscosity, *J. Geophys. Res.* 106 (2001) 6747–6759.
- [41] U.R. Christensen, A.W. Hofmann, Segregation of subducted oceanic crust and the convecting mantle, *J. Geophys. Res.* 99 (1994) 19867–19884.
- [42] M. Ogawa, Chemical stratification in a two-dimensional convecting mantle with magmatism and moving plates, *J. Geophys. Res.* 109 (2003) (doi:10.1029/2002JB002205).
- [43] L.H. Kellogg, B. Hager, R. van der Hilst, Compositional stratification in the deep mantle, *Science* 99 (1999) 276–289.
- [44] P.J. Tackley, Strong heterogeneity caused by deep mantle layering, *Geochem. Geophys. Geosyst.* 3 (4) (2002) (doi:10.1029/2001GC000167).
- [45] A. Davaille, Simultaneous generation of hotspots and super-swells by convection in a heterogeneous planetary mantle, *Nature* 402 (1999) 756–760.
- [46] D. Bercovici, S. Karato, Whole-mantle convection and the transition-zone water filter, *Nature* 425 (2003) 39–44.
- [47] T.W. Becker, J.B. Kellogg, R.J. O'Connell, Thermal constraints on the survival of primitive blobs in the lower mantle, *Earth Planet. Sci. Lett.* 171 (1999) 351–365.
- [48] M. Manga, Mixing of heterogeneities in the mantle: effect of viscosity differences, *Geophys. Res. Lett.* 23 (1996) 403–406.
- [49] A. Meibom, D.L. Anderson, The statistical upper mantle assemblage, *Earth Planet. Sci. Lett.* 217 (2003) 123–139.
- [50] J.B. Kellogg, S.B. Jacobsen, R.J. O'Connell, Modeling the distribution of isotopic ratios in geochemical reservoirs, *Earth Planet. Sci. Lett.* 204 (2002) 183–202.
- [51] D. Graham, K.T.M. Johnson, L.D. Priebe, J.E. Lupton, Hotspot-ridge interaction along the Southeast Indian Ridge near Amsterdam and St. Paul Islands: helium isotope evidence, *Earth Planet. Sci. Lett.* 167 (1999) 297–310.
- [52] R.H. Kingsley, J.-G. Schilling, Plume-ridge interaction in the Easter-Salas y Gomez seamount chain–Easter Microplate system: Pb isotope evidence, *J. Geophys. Res.* 103 (1998) 24150–24177.
- [53] J.-G. Schilling, Fluxes and excess temperatures of mantle plumes inferred from their interaction with migrating mid-ocean ridges, *Nature* 352 (1991) 397–403.

- [54] D. Fontignie, J.-G. Schilling, Mantle heterogeneities beneath the South Atlantic: a Nd–Sr–Pb isotope study along the Mid-Atlantic Ridge (3°S–46°S), *Earth Planet. Sci. Lett.* 142 (1996) 209–221.
- [55] J. Mahoney, A.P. le Roex, Z. Peng, R.L. Fisher, J.H. Natland, Southwestern limits of Indian Ocean ridge mantle and the origin of low $^{206}\text{Pb}/^{204}\text{Pb}$ mid-ocean ridge basalt: isotope systematics of the central southwest Indian Ridge (17°–50° E), *J. Geophys. Res.* 97 (1992) 19771–19790.
- [56] T. Kogiso, M.M. Hirschmann, P.W. Reiners, Length scales of mantle heterogeneities and their relationship to ocean island basalt geochemistry, *Geochim. Cosmochim. Acta* 68 (2) (2004) 345–360.
- [57] J. Phipps Morgan, Thermodynamics of pressure release melting of a veined plum pudding mantle, *Geochem. Geophys. Geosyst.* 2 (2001) (2000GC000049).
- [58] R.A. Keller, M.R. Fisk, W.M. White, Isotopic evidence for late Cretaceous plume-ridge interaction at the Hawaiian hotspot, *Nature* 405 (2000) 673–676.
- [59] B.B. Hanan, J.-G. Schilling, Easter Microplate evolution: Pb isotope evidence, *J. Geophys. Res.* 94 (1989) 7432–7448.
- [60] M. Regelous, A.W. Hofmann, W. Abouchami, S.J.G. Galer, Geochemistry of lavas from the Emperor Seamounts, geochemical evolution of Hawaiian magmatism from 85 to 42 Ma, *J. Petrol.* 44 (2003) 113–140.
- [61] J.G. Fitton, A.D. Saunders, P.D. Kempton, B.S. Hardarson, Does depleted mantle form an intrinsic part of the Iceland plume? *Geochem. Geophys. Geosyst.* 4 (3) (2003) 1032.
- [62] A. Zindler, S. Hart, Chemical geodynamics, *Annu. Rev. Earth Planet. Sci.* 14 (1986) 493–571.
- [63] J. Eisele, M. Sharma, S.J.G. Galer, J. Blichert-Toft, C.W. Devey, A.W. Hofmann, The role of sediment recycling in EM-1 inferred from Os, Pb, Hf, Nd, Sr, isotope and trace elements systematics of the Pitcairn hotspot, *Earth Planet. Sci. Lett.* 196 (2002) 197–212.
- [64] J.D. Woodhead, C.W. Devey, Geochemistry of the Pitcairn seamounts. I: source character and temporal trends, *Earth Planet. Sci. Lett.* 116 (1993) 81–99.
- [65] C. Dupey, P. Vidal, R. Maury, G. Guille, Basalts from Mururoa, Fangataufa and Gambier islands (French Polynesia): geochemical dependence on the age of the lithosphere, *Earth Planet. Sci. Lett.* 117 (1993) 89–100.
- [66] Y. Niu, M. Regelous, I.J. Wendt, R. Batiza, M.J. O'Hara, Geochemistry of near-EPR seamounts: importance of source vs. process and the origin of enriched mantle component, *Earth Planet. Sci. Lett.* 199 (2002) 327–345.
- [67] J.M. Rhodes, S.R. Hart, Episodic trace element and isotopic variations in historical Mauna Loa lavas: implications for magma and plume dynamics, in: J.M. Rhodes, J.P. Lockwood (Eds.), *Mauna Loa Revealed*, Geophysical Monograph, vol. 92, Am. Geophys. Union, Washington, DC, 1995, pp. 263–288.
- [68] M.D. Feigensen, Geochemistry of Kauai volcanics and a mixing model for the origin of Hawaiian alkali basalts, *Contrib. Mineral. Petrol.* 87 (1984) 109–119.
- [69] C.-Y. Chen, F.A. Frey, Origin of Hawaiian tholeiites and alkali basalts, *Nature* 302 (1983) 785–789.
- [70] J. Caplan-Auerbach, F. Duennebier, G. Ito, Origin of intraplate volcanoes from guyot heights and oceanic paleodepth, *J. Geophys. Res.* 105 (2000) 2679–2698.
- [71] S.-S. Sun, W.F. McDonough, Chemical and isotopic systematics of oceanic basalts: implications for mantle composition and processes, in: A.D. Saunders, M.J. Norry (Eds.), *Magmatism in the Ocean Basins*, Special Publication - Geological Society of London, vol. 42, 1989, pp. 313–345.
- [72] R.L. Rudnick, D.M. Fountain, Nature and composition of the continental crust: a lower crustal perspective, *Rev. Geophys.* 33 (3) (1995) 267–309.
- [73] C. Jaupart, J.-C. Mareschal, Constraints on crustal heat production from heat flow data, in: R.L. Rudnick (Ed.), *Treatise on Geochemistry*, vol. 3, 2004, pp. 65–84.
- [74] C.A. Stein, Heat flow of the Earth, in: T.A. Ahrens (Ed.), *Global Earth Physics: a Handbook of Physical Constants*, American Geophysical Union, Washington, DC, 1995, pp. 144–158.
- [75] D.W. Graham, Noble gas isotope geochemistry of mid-ocean ridge and ocean island basalts: characterization of mantle source reservoirs, in: D. Porcelli, C.J. Ballentine, R. Wieler (Eds.), *Noble Gases in Geochemistry and Cosmochemistry*, Reviews in Mineralogy and Geochemistry, Mineral. Soc. Amer., Washington, DC, 2002, pp. 247–318.
- [76] H.J.B. Dick, H. Schouten, An ultraslow-spreading class of ocean ridge, *Nature* 426 (2003) 405–412.
- [77] P.J. Michael, C.H. Langmuir, H.J.B. Dick, J.E. Snow, S.L. Goldstein, D. Graham, K. Lehnert, G. Kurras, W. Jokat, R. Muhe, H.N. Edmonds, Magmatic and amagmatic seafloor generation at the ultraslow-spreading Gakkel ridge, Arctic Ocean, *Nature* 423 (2003) 956–961.
- [78] J.J. Standish, S.R. Hart, H.J.B. Dick, Mantle heterogeneity beneath the Southwest Indian Ridge (9°–25° E), *EOS Trans. AGU* 84 (46) (2003) (Fall Meet. Suppl., Abstract V12C-0611).
- [79] J.-G. Schilling, Upper mantle heterogeneities and dynamics, *Nature* 314 (1985) 62–67.
- [80] G. Ito, Y. Shen, G. Hirth, C. Wolfe, Mantle flow, melting, and dehydration of the Iceland mantle plume, *Earth Planet. Sci. Lett.* 165 (1999) 81–96.
- [81] D.J. DePaolo, J.G. Bryce, A. Dodson, D.L. Shuster, B.M. Kennedy, Isotopic evolution of Mauna Loa and the chemical structure of the Hawaiian plume, *Geochem. Geophys. Geosyst.* 2 (2001) (2000GC000139).
- [82] B.B. Hanan, J.-G. Schilling, The dynamic evolution of the Iceland mantle plume: the lead isotope perspective, *Earth Planet. Sci. Lett.* 151 (1997) 43–60.